Journal of
Materials Chemistry C

PAPER

View Article Online
View Journal | View Issue

Cite this: *J. Mater. Chem. C*, 2014, **2**, 4320

Aggregation-induced emission, mechanochromism and blue electroluminescence of carbazole and triphenylamine-substituted ethenes†

Carrie Y. K. Chan,[a] Jacky W. Y. Lam,[a] Zujin Zhao,[b] Shuming Chen,[c] Ping Lu,[d] Herman H. Y. Sung,[a] Hoi Sing Kwok,[c] Yuguang Ma,[d] Ian D. Williams[a] and Ben Zhong Tang*[abef]

Received 15th January 2014
Accepted 18th March 2014

DOI: 10.1039/c4tc00097h

www.rsc.org/MaterialsC

Carbazole and triphenylamine-substituted ethenes are synthesized [$Ph_2C{=}CPh(R)$, R = 9-carbazolyl, 9-hexyl-3-carbazolyl and 4-(diphenylamino)phenyl] and their optical properties are investigated. All luminogens are nonemissive when molecularly dissolved in good solvents but become highly emissive in the aggregated state, showing a phenomenon of aggregation-induced emission. High solid-state fluorescence quantum yields up to 97.6% have been achieved in their solid thin films. The luminogens are thermally stable, showing high degradation temperatures of up to 315 °C. They exhibit mechanochromism: their emissions can be repeatedly switched between blue and green colors by simple grinding–fuming and grinding–heating processes due to the morphological change from crystalline to amorphous state and *vice versa*. Multilayer light-emitting diodes with device configurations of ITO/NPB/dye/TPBi/Alq_3/LiF/Al, ITO/NPB/dye/TPBi/LiF/Al and ITO/dye/TPBi/LiF/Al are fabricated, which emit sky blue light with maximum luminance, current efficiency, power efficiency and external quantum efficiency of 11 700 cd m^{-2}, 7.5 cd A^{-1}, 7.9 lm W^{-1} and 3.3%, respectively.

Introduction

Since Tang demonstrated the use of organic light emitting diodes (OLEDs) with multilayer structures to improve the device performance, a large number and a wide variety of organic fluorophores have been prepared.[1] In OLEDs, the emitters are fabricated as thin films and their device performance depends somewhat on their solid-state fluorescence quantum yields ($\Phi_{F,F}$). However, many organic fluorophores are non-luminescent or weakly emissive in the solid state, although their dilute solutions emit strongly under UV irradiation. This is attributed to the strong intermolecular electronic interactions in the solid state, which favour the formation of detrimental species such as excimers and exciplexes. Such a phenomenon is coined as "aggregation-caused quenching" (ACQ) and has been a textbook-knowledge.[2] In contrast to a large number of ACQ molecules, examples of highly emissive organic solids with high $\Phi_{F,F}$ values are still rare, especially those with strong solid-state blue emission. It is therefore challenging to achieve stable and efficient solid-state blue emitters compared with green and red emitters as the performance of the current blue OLEDs is still much beyond than those of the green and red ones. With the fact that blue is one of the primary colors, it is essential for the fabrication of full-color displays. In addition, blue-emitting materials may act as host materials for green and red dopants.

Recently, we and other groups observed a novel phenomenon of aggregation-induced emission (AIE) which is exactly opposite to the ACQ effect: a series of propeller-like molecules are practically nonluminescent when molecularly dissolved in good solvents but become highly emissive when aggregated into nanoparticles in poor solvents or fabricated as thin films in the solid state.[3,4] The AIE effect enables the molecules to find high-tech applications as chemical sensors, biological probes, stimuli-responsive nanomaterials and active layers for the fabrication of OLEDs.[5] Among the AIE luminogens, tetraphenylethene (TPE) possesses a simple molecular structure with a splendid AIE effect (Chart 1). However, its EL performance is

---

[a] *Department of Chemistry, Institute for Advanced Study, Institute of Molecular Functional Materials, Division of Life Science, Division of Biomedical Engineering and State Key Laboratory of Molecular Neuroscience, The Hong Kong University of Science & Technology (HKUST), Clear Water Bay, Kowloon, Hong Kong, China. E-mail: tangbenz@ust.hk*

[b] *State Key Laboratory of Luminescent Materials and Devices, South China University of Technology (SCUT), Guangzhou 510640, China*

[c] *Centre for Display Research, The Hong Kong University of Science & Technology, Clear Water Bay, Kowloon, Hong Kong, China*

[d] *State Key Laboratory of Supermolecular Structure and Materials, Jilin University, Changchun 150012, China*

[e] *Guangdong Innovative Research Team, SCUT-HKUST Joint Research Laboratory, South China University of Technology (SCUT), Guangzhou 510640, China*

[f] *HKUST-Shenzhen Research Institute, No. 9 Yuexing 1st RD, South Area, Hi-tech Park, Nanshan, Shenzhen 518057, China*

† Electronic supplementary information (ESI) available: Crystal data of **1–3** and supplementary figures. CCDC 970451–970453. For ESI and crystallographic data in CIF or other electronic format see DOI: 10.1039/c4tc00097h

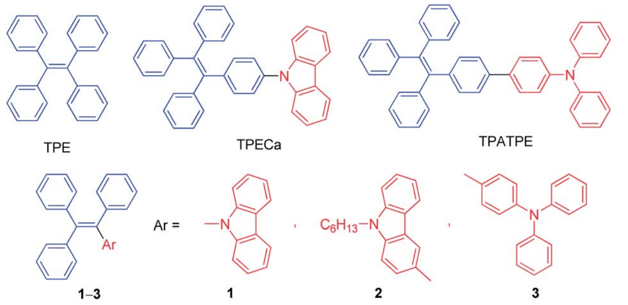

Chart 1 Molecular structures of tetraphenylethene and its derivatives containing carbazole and triphenylamine units.

quite poor with maximum luminance (L_{max}), current efficiency ($\eta_{C,max}$) and external quantum efficiency ($\eta_{ext,max}$) of 1800 cd m^{-2}, 0.45 cd A^{-1} and 0.4%, respectively.[6] Carbazole and triphenylamine (TPA) are well-known hole-transporting materials but suffer from the ACQ effect in the condensed state. Incorporation of TPE into their structures has solved their ACQ problem and meanwhile generates efficient solid-state emitters such as TPECa and TPATPE with unity $\Phi_{F,F}$ values. OLEDs fabricated using TPECa and TPATPE show good device performance. For example, the EL device of TPECa with a configuration of ITO/NPB/TPECa/TPBi/Alq$_3$/LiF/Al exhibits a L_{max} of 7508 cd m^{-2} and $\eta_{ext,max}$ of 1.8%.[7] The performance of the EL device based on TPATPE is more impressive, exhibiting L_{max} and $\eta_{ext,max}$ of 26 090 cd m^{-2} and 3.3%, respectively.[8] Both TPECa and TPATPE can play dual roles as light-emitting and hole-transporting layers in OLEDs. This simplifies the device structure and helps to reduce the fabrication cost.

Mechanochromic luminescent materials, which show emission color or intensity change induced by mechanical stress, have aroused increasing interest in recent years due to their potential applications in many fields such as sensors, displays and memory devices.[9] Taking advantage of their high $\Phi_{F,F}$ values, AIE-active molecules are thus considered as promising candidates for such applications. A variety of AIE luminogens with various functionalities have been prepared. However, AIE molecules with mechanochromic fluorescence properties are seldom reported. With such regard, we designed and synthesized new luminogens from triphenylethene, carbazole and TPA building blocks (**1–3**; Chart 1). Unlike TPECa and TPATPE, the carbazole and TPA units serve as skeletons, rather than substituents, for the construction of **1–3**. Luminogens **1–3** exhibit not only AIE characteristics but also intriguing mechanochromism due to the morphological change from the crystalline to the amorphous state and *vice versa*. Multilayer OLEDs utilizing the new luminogens are fabricated, which show blue light with high luminance and current efficiency up to 11 700 cd m^{-2} and 7.5 cd A^{-1}, respectively.

Results and discussion

Synthesis

To enrich the AIE research and widen its practical applications, we designed the molecular structures of three new AIE luminogens and elaborated a multistep reaction route for their syntheses (Scheme 1). Compound **5** was first prepared by reaction of carbazole (**4**) with benzyl bromide in the presence of tetrabutylammonium bromide under basic conditions. Lithiation of **5** followed by reaction with benzophenone and acid-catalyzed dehydration afforded **1**. On the other hand, the Friedel–Crafts acylation of benzoyl chloride (**7**) with 9-hexylcarbazole and TPA furnished **8a** and **8b**, which were converted into **2** and **3**, respectively, by their reaction with diphenylmethyllithium followed by acid-catalyzed dehydration. All the intermediates and final products were carefully purified and fully characterized by NMR and mass spectroscopy, from which satisfactory analysis data corresponding to their expected molecular structures were obtained. Single crystals of **1–3** were grown from their dichloromethane–methanol solutions and characterized crystallographically. Their ORTPE drawings are shown in Fig. 1 and the associated crystal data are summarized in Table S1 in the ESI.† All the luminogens are soluble in common organic solvents, such as tetrahydrofuran, toluene, dichloromethane and chloroform, but insoluble in water.

Optical properties

The dilute THF solution (10 μM) of **1** exhibits a peak maximum at 341 nm (Fig. 2). The spectra of **2** and **3**, however, are located at longer wavelength, revealing that they possess a better conjugation. Like other AIE luminogens prepared previously, the photoluminescence (PL) spectra of **1–3** in dilute THF solutions (10 μM) exhibit only noisy PL signals with no discernible peak maxima (Fig. 3 and S1 and S2, ESI†). The solution-state fluorescence quantum yields ($\Phi_{F,S}$) of **1** and **2** estimated using 9,10-diphenylanthracene as standard are merely 0.70% and 0.27%, respectively, indicating that they are weak emitters when molecularly dissolved in good solvents. These values are much lower than those of carbazole (37%)[10a] and TPA (13.0),[10b]

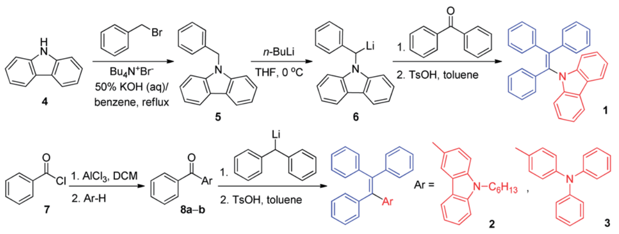

Scheme 1 Synthesis routes to carbazole and triphenylamine-substituted ethenes.

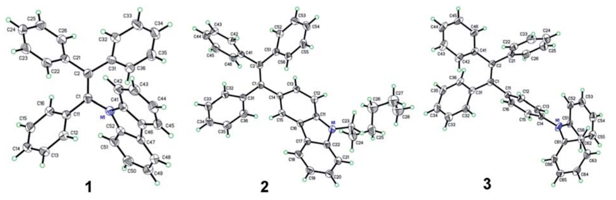

Fig. 1 ORTEP drawings of **1–3** (CCDC 970451–970453).

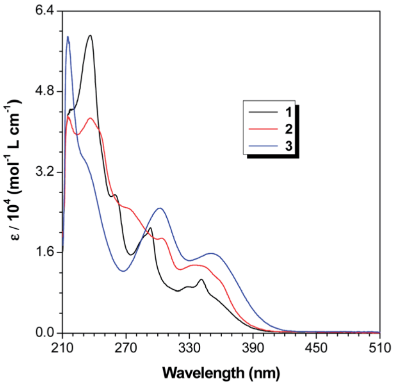

Fig. 2 UV spectra of **1–3** in THF solutions. Solution concentration: 10^{-5} M.

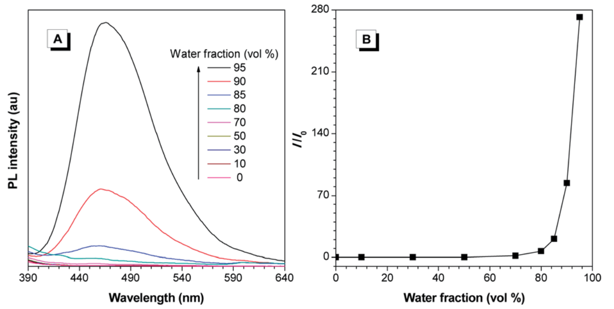

Fig. 3 (A) PL spectra of **1** in THF and THF–H_2O mixtures with different water fractions. Concentration: 10^{-5} M; excitation wavelength: 340 nm. (B) Plot of I/I_0 values *versus* compositions of the THF–H_2O mixtures of **1**.

suggesting that the triphenylvinyl unit in **1–3** works as a PL quencher in the solution state.

Whereas luminogens **1–3** are almost non-fluorescent in solutions, they emit intensely in the aggregated state. As shown in Fig. 3, the PL intensity of **1** remains low in aqueous mixtures with less than 80% water content but starts to increase swiftly afterwards. The emission intensity reaches its maximum at 95% water fraction. From the pure THF solution to the THF–H_2O mixture with 90% water content, the PL intensity rises by 350-fold. Similar phenomena are also observed in **2** and **3** (Fig. S1 and S2†). Clearly, the emissions of **1–3** are induced by aggregate formation, or in other words, they are AIE-active. In dilute solution, the rotation of multiple phenyl rings has consumed the energy of the excitons through the nonradiative relaxation channel and thus has quenched the light emission of the dye molecules. In the aggregate state, the intramolecular rotation (IMR) is restricted, thus allowing the luminogens to emit intensely. We further investigated the PL behaviors of **1–3** in the solid state. The emissions of their thin films are observed at 465–500 nm, which are similar to the PL of their aggregates in THF–H_2O mixtures (Table 1). The $\Phi_{F,F}$ value of **3** (97.6%) measured using a calibrated integrating sphere is much higher than those of **1** and **2** (55.7% for **1** and 33.1% for **2**), presumably due to its higher conjugation.

Table 1 Absorption and emission of **1–3** in the solution (soln)[a], aggregated (aggr)[b], crystalline (cryst) and amorphous (amor)[c] states

	λ_{ab}[d] (nm)	λ_{em}[e] (nm)			
Luminogen	Soln	Soln ($\Phi_{F,S}$)	Aggr	Cryst	Amor ($\Phi_{F,F}$)
1	341	(0.70)	466	455	465 (55.7)
2	342	(0.27)	489	454	490 (33.1)
3	350	(1.22)	499	429	500 (97.6)

[a] In dilute THF solution (10 μM). [b] In the THF–H_2O mixture (1 : 9 by volume). [c] In a solid thin film. [d] Absorption maximum. [e] Emission maximum with the quantum yield (%) given in the parentheses. $\Phi_{F,S}$ = fluorescence quantum yield in THF solution determined using 9,10-diphenylanthracene (Φ_F = 90% in cyclohexane) as standard. $\Phi_{F,F}$ = fluorescence quantum yield for the thin film measured by a calibrated integrating sphere.

To gain deep insight into the optical behaviors of the luminogens, we performed theoretical calculations on their energy levels. Their highest occupied (HOMO) and lowest unoccupied molecular orbitals (LUMO) plots are given in Fig. 4. The triphenylvinyl units are twisted from the plane of the carbazole or TPA unit in all the molecules, which prevents emission quenching caused by the unfavourable π–π stacking interaction. Whereas the HOMO of **1** and **2** are dominated by the orbitals from the carbazole ring and part of the triphenylvinyl unit, the orbitals of their LUMO are located mainly on the latter one. On the other hand, the electron cloud of the HOMO of **3** is located mainly on the TPA unit. However, it shows almost no contribution to the LUMO energy level. The calculated band gaps for **1–3** are 3.80, 3.85 and 3.61 eV, respectively.

Interestingly, the crystals of **1–3** emit at 429–455 nm, which are 10–71 nm blue-shifted from those of the amorphous films. The unusual blue shift observed in the crystalline phase may be attributable to the conformation twisting of the aromatic rings

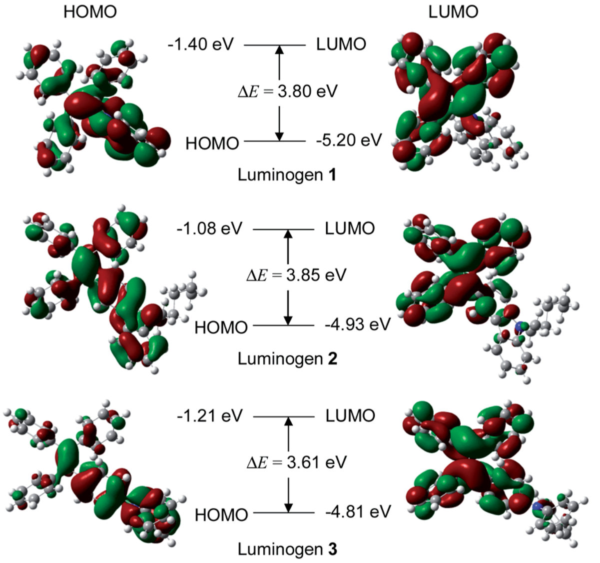

Fig. 4 Molecular orbital amplitude plots of HOMO and LUMO levels of **1–3** calculated using the B3LYP/6-31G* basis set.

of the luminogens in order to fit into the crystalline lattices. Without such restraint, the molecules in the amorphous state may assume a more planar conformation and thus show redder luminescence. To gain further insight into the AIE mechanism, we checked the geometric structures and packing arrangements of **1** and **3** in the crystalline state. As shown in Fig. 5, multiple C–H⋯π hydrogen bonds with distances of 2.620 and 3.075 Å are formed between the carbazolyl protons of one molecule of **1** and the π cloud of the carbazole unit of the neighbouring molecule. Similar interactions are also observed in **3**. These multiple C–H⋯π hydrogen bonds help rigidify the molecular conformation and have locked the molecular rotation. As a result, the excited state energy consumed by the IMR process is greatly reduced, thus enabling **1** and **3** to emit intensely in the solid state. The dihedral angles between the vinyl core and the carbazole or triphenylamine unit are 43.7°, 46.1° and 53.0° for **1–3**, respectively. This suggests that **3** takes a more twisted conformation, thus leading to bluer crystal emission and the largest hypochromic PL shift from aggregated to crystal state.

Upon gently grinding the crystals of **3** using a spatula or pestle, their emission changes from blue to green (Fig. 6), demonstrating a property of mechanochromic fluorescence. Since the PL of the mechanically agitated crystals is close to that of the amorphous film (Fig. 7A), such a phenomenon should be associated with the morphological change from crystalline to amorphous state. This is supported by the result from powder X-ray diffraction analysis: whereas the diffractogram of the crystals exhibits many sharp peaks, that of the mashed crystals shows fewer and broader peaks with much weaker intensities, indicating that they, to a large extent, are of amorphous nature (Fig. S3†). After solvent fuming to acetone vapour at room temperature for 10 min or heating at 120 °C in air for 10 min, the green powders recrystallize and are restored nearly to the blue form. The switching between the blue crystalline and green amorphous states of **3** can be repeated for many cycles without fatigue because this process is nondestructive in nature (Fig. 7B). We believe that by applying a larger pressure load using a hydraulic presser, a more drastic fluorescence shift can be observed. The change in reflectivity has been commonly used as an output in rewritable optical media. A luminescence-based process is of advantage because it offers higher sensitivity, lower background noise and potential for two-dimensional imaging.[11] Luminogen **3** is thus a promising candidate for innovative applications in optical information storage systems.

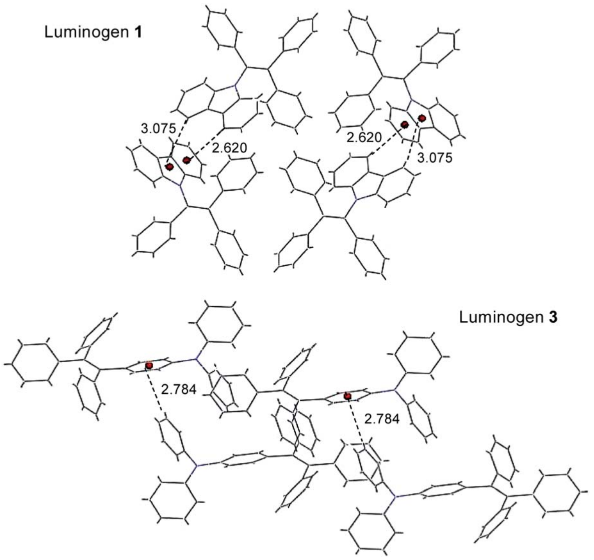

Fig. 5 Perspective view of the packing arrangements in crystals of **1** and **3**. The aromatic C–H⋯π hydrogen bonds are denoted by dotted lines.

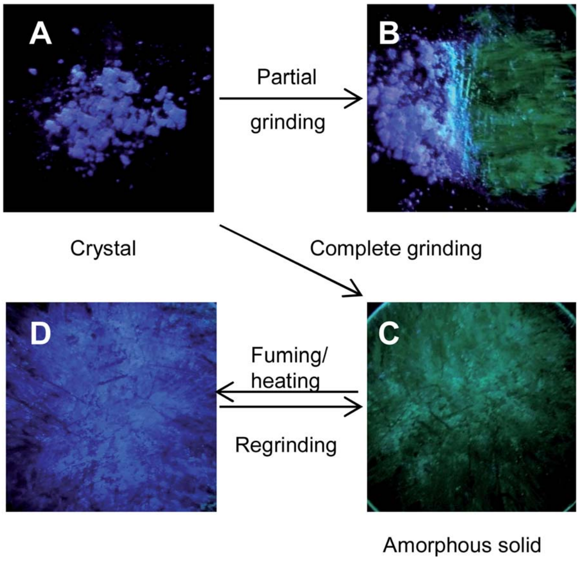

Fig. 6 Reversibly switching between the blue crystalline and green amorphous states of **3** by grinding–fuming and grinding–heating cycles. The photographs were taken under 365 nm UV irradiation from a hand-held UV lamp.

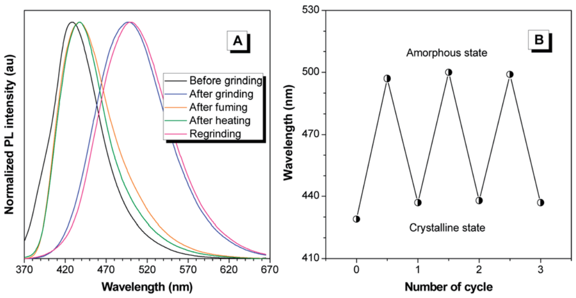

Fig. 7 (A) Change in the PL spectrum of crystals of **3** by grinding–fuming and grinding–heating processes. (B) Repeated switching of the light emission of **3** by the grinding–fuming cycle.

Thermal properties

The thermal stability of **1–3** was evaluated by thermogravimetric analysis (TGA) under nitrogen at a heating rate of 10 °C min^{-1}. As shown in Fig. 8, all the luminogens are thermally stable, losing 5% of their weights at temperatures (T_d) from 294 to 315 °C. Their thermal transitions were investigated by differential scanning calorimetry (DSC) at a heating rate of

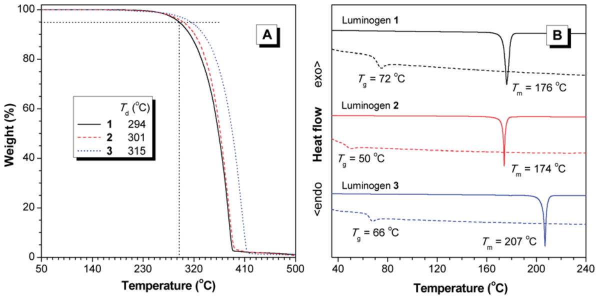

Fig. 8 (A) TGA curves and (B) DSC thermograms of first (solid lines) and second (dotted lines) heating scans of **1–3** recorded under nitrogen at a heating rate of 10 °C min.

10 °C min^{-1}. All the compounds exhibited clear melting transitions (T_m) in the range of 174–207 °C. They also possess good morphological stability, as suggested by their reasonably high glass-transition temperatures (T_g) of 72, 50 and 66 °C, respectively. Coupled with their efficient solid-state emission, luminogens **1–3** are thus promising EL materials.

Electroluminescence

The efficient light emission and high thermal stability of **1–3** encourage us to investigate their electroluminescence (EL) properties. Multilayer OLEDs with configurations of ITO/NPB (50 nm)/LEL (20 nm)/TPBi (30 nm)/Alq_3 (20 nm)/LiF (1 nm)/Al (100 nm) (Device I) and ITO/NPB (50 nm)/LEL (20 nm)/TPBi (30 nm)/LiF (1 nm)/Al (100 nm) (Device II) were constructed, where luminogens **1–3** worked as the light-emitting layer (LEL), NPB functioned as the hole-transporting material, TPBi served as the electron-transporting and/or hole-blocking layer and Alq_3 worked as the electron-transporting material, respectively. The performance and EL data are depicted and summarized in Fig. 9 and Table 2. Devices I of **1–3** emit bright sky blue EL at 468–488 nm, which are close to the PL spectra of their amorphous thin films. This indicates that both EL and PL originate from the same radiative decay of the singlet excitons. Among the luminogens, the OLED based on **3** shows the best performance. The device is turned on at a low voltage of 3.2 V and exhibits an L_{max} of 7140 cd m^{-2}. The $\eta_{C,max}$, maximum power efficiency ($\eta_{P,max}$) and $\eta_{ext,max}$ attained by the device are 7.5 cd A^{-1}, 7.9 lm W^{-1} and 3.3%, respectively. Compared to previous results obtained from other AIE luminogens, these values are pretty high. Removal of the Alq_3 layer in Device I forms Device II, which results in different consequences. Whereas the EL performance of Device II of **1** is slightly better than that of Device I, those of **2** and **3** become poorer though the EL devices exhibit higher L_{max} values.

Materials with multi-functional properties, such as light-emitting and hole- and/or electron-transporting capabilities, are more useful for technological applications and in great demand because they can greatly simplify the device structure and reduce the fabrication cost. Carbazole and TPA are well-known for their light-emitting and hole-transporting properties. Since luminogens **1–3** are constructed from these moieties, they may serve as bifunctional materials. To test such possibility, OLEDs with a configuration of ITO/LEL/TPBi (40 nm)/LiF (1 nm)/Al (100 nm) are constructed, where **1–3** served as both light-emitting and hole-transporting layers. Again, luminogen **3** shows the best EL performance. Its EL device emits at 488 nm, showing an L_{max}, $\eta_{C,max}$, $\eta_{P,max}$ and $\eta_{ext,max}$ of 11 700 cd m^{-2}, 2.4 cd A^{-1}, 1.0 lm W^{-1} and 1.1%, respectively (Fig. 10). These values, however, are much inferior to those of Device I and II, leaving much room for further improvement. Nevertheless, the EL data given in Table 2 demonstrate the great potential of the present luminogens as solid light-emitters for the construction of efficient EL devices.

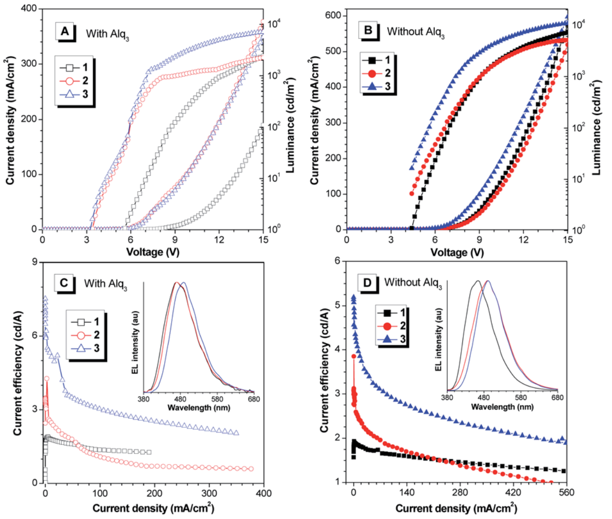

Fig. 9 Plots of (A and B) current density and luminance *versus* voltage and (C and D) current efficiency *versus* current density in the multilayer light-emitting diode of **1–3** with device configurations of (A and C) ITO/NPB/LEL/TPBi/Alq_3/LiF/Al and (B and D) ITO/NPB/LEL/TPBi/LiF/Al. The inset in (C) and (D): EL spectra of **1–3**.

Table 2 EL performance of **1–3**[a]

Dye	λ_{EL} (nm)	V_{on} (V)	L_{max} (cd m^{-2})	$\eta_{P,max}$ (lm W^{-1})	$\eta_{C,max}$ (cd A^{-1})	$\eta_{ext,max}$ (%)
Device I: ITO/NPB/LEL/TPBi/Alq_3/LiF/Al						
1	468	5.6	2410	0.8	1.9	1.0
2	468	3.4	2240	3.2	4.3	1.8
3	488	3.2	7140	7.9	7.5	3.3
Device II: ITO/NPB/LEL/TPBi/LiF/Al						
1	472	4.4	7160	1.2	1.9	1.3
2	492	4.4	5130	2.0	3.9	1.7
3	492	4.0	10 900	3.7	5.2	3.1
Device III: ITO/LEL/TPBi/LiF/Al						
1	488	4.0	6300	0.4	1.1	0.6
2	492	4.6	4390	0.5	1.0	0.4
3	488	1.0	11 700	1.0	2.5	1.1

[a] Abbreviation: LEL = light-emitting layer, λ_{EL} = electroluminescence maximum, V_{on} = turn-on voltage at 1 cd m^{-2}, L_{max} = maximum luminance, $\eta_{P,max}$ = maximum power efficiency, $\eta_{C,max}$ = maximum current efficiency and $\eta_{ext,max}$ = maximum external quantum efficiency.

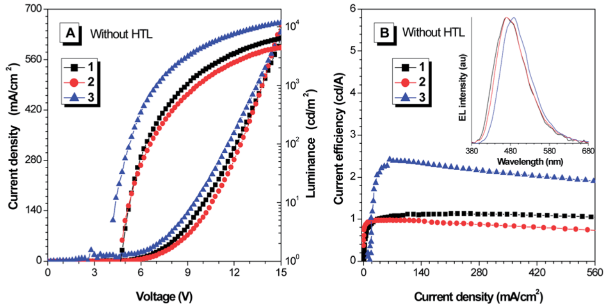

Fig. 10 Plots of (A) current density and luminance *versus* voltage and (B) current efficiency *versus* current density in the multilayer light-emitting diode of **1–3** with a device configuration of ITO/LEL/TPBi/LiF/Al. The inset in (B): EL spectra of **1–3**.

Conclusions

In this work, we designed and synthesized a group of carbazole and triphenylamine-substituted ethenes (**1–3**). All the luminogens are well characterized by spectroscopic techniques and their chemical structures are further confirmed by X-ray crystallography. Whereas they are nonemissive in dilute THF solutions, they become strong emitters when aggregated in poor solvents or fabricated as films in the solid state, demonstrating the phenomenon of AIE. These luminogens exhibit high solid-state fluorescence quantum yields of up to 97.6% and enjoy high thermal stability (T_d up to 315 °C). They also show intriguing mechanochromic fluorescence properties: their emission can be repeatedly switched between blue and green colors by simple grinding–fuming and grinding–heating processes due to the morphological change from crystalline to amorphous state and *vice versa*. OLEDs using **1–3** as emitters are fabricated, which show high luminance and current and external quantum efficiencies of up to 11 700 cd m^{-2}, 7.5 cd A^{-1} and 3.3%, respectively.

Experimental section

Materials and instrumentation

Dichloromethane (DCM) and tetrahydrofuran (THF) were distilled from calcium hydride and sodium benzophenone ketyl, respectively, under nitrogen immediately prior to use. All the chemicals and reagents were purchased from Aldrich and used as received without further purification. ^{1}H and ^{13}C NMR spectra were recorded on a Bruker AV 300 spectrometer in deuterated chloroform using tetramethylsilane (TMS; $\delta = 0$) as the internal reference. High resolution mass spectra (HRMS) were recorded on a GCT premier CAB048 mass spectrometer operating in MALDI-TOF mode. UV spectra were recorded on a Milton Roy Spectronic 3000 Array spectrophotometer. Photoluminescence (PL) was recorded on a Perkin-Elmer LS 55 spectrofluorometer. Thermogravimetric analysis (TGA) was carried out on a TA TGA Q5000 analyzer under nitrogen at a heating rate of 10 °C min^{-1}. The thermal transitions of the luminogens were investigated by differential scanning calorimetry (DSC) using a TA DSC Q1000 analyzer under dry nitrogen at a heating rate of 10 °C min^{-1}. Single crystal X-ray diffraction intensity data were collected at 100 K on a Bruker–Nonices Smart Apex CCD diffractometer with graphite monochromated Mo Kα radiation. Processing of the intensity data was carried out using the SAINT and SADABS routines and the structure and refinement were conducted using the SHELTL suite of X-ray programs (version 6.10). The ground-state geometries were optimized using the density functional (DFT) with B3LYP hybrid functional at the basis set level of 6-31G*. All the calculations were performed using the Gaussian 03 package.

Device fabrication

The devices were fabricated on 80 nm-ITO coated glasses with a sheet resistance of 25 Ω □$^{-1}$. Prior to loading into the pretreatment chamber, the ITO-coated glasses were soaked in an ultrasonic detergent for 30 min, followed by spraying with de-ionized water for 10 min, soaking in ultrasonic de-ionized water for 30 min and oven-baking for 1 h. The cleaned samples were treated with perfluoromethane plasma with a power of 100 W, gas flow of 50 sccm and pressure of 0.2 Torr for 10 s in the pretreatment chamber. The samples were transferred to the organic chamber with a base pressure of 7 × 10^{-7} Torr for the deposition of *N*,*N*-bis(1-naphthyl)-*N*,*N*-diphenylbenzidine (NPB), emitter, 2,2′,2′′-(1,3,5-benzinetriyl)tris(1-phenyl-1-*H*-benzimidazole) (TPBi) and/or tris(8-hydroxyquinolinato) aluminium (Alq$_3$) which served as hole-transporting, light-emitting and hole-blocking and electron-transporting layers, respectively. The samples were then transferred to the metal chamber for cathode deposition which composed of lithium fluoride (LiF) capped with aluminium (Al). The light-emitting area was 4 mm^2. The current density–voltage characteristics of the devices were measured on a HP4145B semiconductor parameter analyzer. The forward direction photons emitted from the devices were detected by a calibrated UDT PIN-25D silicon photodiode. The luminance and external quantum efficiencies of the devices were inferred from the photocurrent of the photodiode. The EL spectra were obtained using a PR650 spectrophotometer. All the measurements were carried out under air at room temperature without device encapsulation.

Preparation of nanoaggregates

Stock THF solutions of the compounds with a concentration of 10^{-3} M were prepared. Aliquots of the stock solutions were transferred to 10 mL volumetric flasks. After adding appropriate amounts of THF, water was added dropwise under vigorous stirring to furnish 10^{-5} M solutions with different water contents (0–95 vol%). The PL measurements of the resulting solutions were then performed immediately.

Synthesis

Synthesis of 9-benzylcarbazole (5). Into a 100 mL one-necked round bottom flask were added carbazole (**4**, 3 g, 17.9 mmol), benzyl bromide (2.56 g, 15.0 mmol), tetrabutylammonium bromide (0.48 g, 0.15 mmol), 50 wt% of aqueous KOH solution (30 mL) and benzene (30 mL). The reaction mixture was heated to reflux overnight. After being cooled to room temperature, the reaction mixture was extracted with DCM. The organic layer was washed with water and dried over magnesium sulfate. After filtration and solvent evaporation, the crude product was purified by silica-gel column chromatography using hexane as eluent. A white solid of **5** was obtained in 88.1% yield (3.39 g). ^{1}H NMR (300 MHz, $CDCl_3$), δ (ppm): 8.13 (d, 2H), 7.45–7.37 (m, 4H), 7.35–7.23 (m, 5H), 7.14 (d, 2H), 5.51 (s, 2H); ^{13}C NMR (75 MHz, $CDCl_3$), δ (ppm): 141.33, 137.85, 129.44, 128.12, 127.08, 126.51, 123.69, 121.06, 119.87, 109.56, 47.23; HRMS (MALDI-TOF): *m*/*z* 257.1220 [M^+, calcd 257.1204].

1-(9-Carbazolyl)-1,2,2-triphenylethene (1). To a solution of **5** (1.2 g, 4.66 mmol) in dry THF (40 mL) was added 4.44 mmol of *n*-butyllithium solution (2.5 M in hexane) at 0 °C under nitrogen. The resulting solution containing **6** was stirred at 0 °C and 4.44 mmol of benzophenone was then added. The reaction mixture was allowed to warm to room temperature and stirred for another 6 h. The reaction was quenched by adding an aqueous solution of ammonium chloride. The organic layer was extracted with DCM three times. The resulting organic layers were combined, washed with water and dried over anhydrous magnesium sulfate. After solvent evaporation, the crude alcohol (containing excess diphenylmethane) was dissolved in about 50 mL of toluene in a 100 mL two-necked round bottom flask equipped with a condenser. A catalytic amount of *p*-toluenesulphonic acid (TsOH) was then added and the mixture was heated to reflux. After being cooled to room temperature, the organic layer was washed with 25 mL of 10% aqueous sodium bicarbonate solution twice and dried over anhydrous magnesium sulfate. After solvent evaporation, the crude product was purified by silica gel column chromatography using hexane–DCM (4 : 1 v/v) as eluent. White solid; yield 40.0% (0.75 g). ^{1}H NMR (300 MHz, $CDCl_3$), δ (ppm): 7.98 (d, 2H), 7.27–7.22 (m, 10H), 7.17–7.03 (m, 3H), 7.02–7.01 (m, 3H), 6.91–6.86 (m, 5H). ^{13}C NMR (75 MHz, $CDCl_3$), δ (ppm): 142.27, 142.23, 142.12, 141.01, 138.30, 132.66, 132.20, 130.54, 129.33, 128.91, 128.76, 128.56, 128.37, 128.17, 128.12, 126.29, 124.06, 120.63, 120.29, 111.52. HRMS (MALDI-TOF): *m*/*z* 421.1860 [M^+, calcd 421.1830].

(9-Hexyl-3-carbazolyl)(phenyl)methanone (8a). 9-Hexylcarbazole was first prepared from carbazole (**4**, 5 g, 29.9 mmol), 1-bromohexane (4.11 g, 24.9 mmol) and tetrabutylammonium bromide (0.80 g, 2.5 mmol) in 50 wt% of aqueous KOH solution (40 mL) and benzene (40 mL). The procedures were similar to those for the synthesis of **5**. Viscous colourless liquid; yield 90.0% (5.66 g). ^{1}H NMR (300 MHz, $CDCl_3$), δ (ppm): 8.10 (d, 2H), 7.46–7.38 (m, 4H), 7.22 (t, 2H), 4.28 (t, 2H), 1.90–1.80 (m, 2H), 1.50–1.24 (m. 6H), 0.86 (t, 3H). ^{13}C NMR (75 MHz, $CDCl_3$), δ (ppm): 141.08, 126.22, 123.46, 121.00, 119.33, 109.31, 43.74, 32.27, 29.61, 27.66, 23.23, 14.71. HRMS (MALDI-TOF): *m*/*z* 251.1683 [M^+, calcd 251.1674].

Into another 100 mL one-necked round bottom flask were added 9-hexyl-carbazole (2 g, 7.96 mmol), benzoyl chloride (**7**, 1.12 g, 7.96 mmol), aluminium chloride (1.11 g, 8.35 mmol) and DCM (40 mL). The reaction mixture was stirred overnight. A large amount of cold water was added to quench the reaction and the reaction mixture was then extracted with DCM. The organic layer was washed with water and dried over magnesium sulfate. After filtration and solvent evaporation, the crude product was purified by silica-gel column chromatography using hexane–DCM (3 : 2 v/v) as eluent. White solid; yield 84.2% (2.38 g). ^{1}H NMR (300 MHz, $CDCl_3$), δ (ppm): 8.60 (s, 1H), 8.10 (d, 1H), 8.04 (d, 1H), 7.84 (d, 2H), 7.60–7.43 (m, 6H), 7.26 (t, 1H), 4.33 (t, 2H), 1.94–1.84 (m, 2H), 1.42–1.23 (m, 6H), 0.87 (t, 3H). ^{13}C NMR (75 MHz, $CDCl_3$), δ (ppm): 197.30, 143.70, 141.78, 139.71, 132.31, 130.57, 129.09, 128.84, 127.08, 124.72, 123.77, 123.08, 121.38, 120.57, 109.89, 108.94, 44.03, 32.20, 29.59, 27.60, 23.20, 14.68. HRMS (MALDI-TOF): *m*/*z* 355.1933 [M^+, calcd 355.1936].

[4-(Diphenylamino)phenyl](phenyl)methanone (8b). Compound **8b** was prepared from triphenylamine (2 g, 8.15 mmol), benzoyl chloride (1.15 g, 8.15 mmol) and aluminium chloride (1.14 g, 8.55 mmol) in DCM (40 mL). The procedures were similar to those for the synthesis of **8a**. Green solid; yield 80.1% (2.28 g). ^{1}H NMR (300 MHz, $CDCl_3$), δ (ppm): 7.77 (d, 2H), 7.71 (d, 2H), 7.55 (t, 1H), 7.46 (t, 2H), 7.33 (t, 4H), 7.19–7.12 (m, 6H), 7.03 (t, 2H). ^{13}C NMR (75 MHz, $CDCl_3$), δ (ppm): 195.91, 152.60, 147.17, 139.14, 132.65, 132.38, 130.33, 130.29, 130.20, 128.80, 126.67, 125.32, 120.20. HRMS (MALDI-TOF): *m*/*z* 349.1465 [M^+, calcd 349.1467].

1-(9-Hexyl-3-carbazolyl)-1,2,2-triphenylethene (2). To a solution of diphenylmethane (0.50 g, 2.95 mmol) in dry THF (30 mL) was added 2.81 mmol of *n*-butyllithium solution (2.5 M in hexane) at 0 °C under nitrogen. The resulting solution containing diphenylmethyllithium was stirred at 0 °C and 2.81 mmol of **8a** was then added. The procedures were similar to those for the synthesis of **1**. White solid; yield 42.9% (0.61 g). ^{1}H NMR (300 MHz, $CDCl_3$), δ (ppm): 7.87 (d, 1H), 7.75 (s, 1H), 7.40 (d, 1H), 7.35 (d, 1H), 7.17–7.02 (m, 18H), 4.21 (t, 2H), 1.85–1.82 (m, 2H), 1.38–1.29 (m, 6H), 0.88 (t, 3H). ^{13}C NMR (75 MHz, $CDCl_3$), δ (ppm): 145.20, 144.98, 142.39, 141.28, 140.62, 139.91, 135.12, 132.27, 132.17, 132.16, 130.28, 129.19, 128.81, 128.29, 128.23, 126.96, 126.81, 126.74, 126.52, 126.06, 124.01, 123.56, 122.97, 120.98, 119.31, 109.30, 108.37, 43.79, 32.22, 29.60, 27.65, 23.24, 14.70. HRMS (MALDI-TOF): *m*/*z* 505.3439 [M^+, calcd 505.2770].

1-[(4-Diphenylamino)phenyl]-1,2,2-triphenylethene (3). To a solution of diphenylmethane (0.45 g, 2.70 mmol) in dry THF (40 mL) was added 2.58 mmol of *n*-butyllithium solution (2.5 M in hexane) at 0 °C under nitrogen. The resulting solution containing diphenylmethyllithium was stirred at 0 °C and 2.58 mmol of **8b** was then added. The procedures were similar to those for the synthesis of **1**. White solid; yield 38.8% (0.50 g). ^{1}H NMR (300 MHz, $CDCl_3$), δ (ppm): 7.25–7.21 (m, 4H), 7.19–7.02 (m, 21H), 6.85 (d, 2H), 6.79 (d, 2H). ^{13}C NMR (75 MHz, $CDCl_3$), δ (ppm): 148.28, 146.65, 144.73, 144.47, 144.27, 141.38, 141.16, 138.60, 132.84, 132.06, 129.80, 129.20, 128.82, 128.28, 127.10, 127.01, 124.90, 123.47, 123.35. HRMS (MALDI-TOF): *m*/*z* 499.2428 [M^+, calcd 499.2300].

Acknowledgements

This work was partially supported by the National Basic Research Program of China (973 Program; 2013CB834701), the Research Grants Council of Hong Kong (HKUST2/CRF/10 and N_HKUST620/11), the Innovation and Technology Commission

(ITCPD/17-9) and the University Grants Committee of Hong Kong (AoE/P-03/08 and T23-713/11-1). B.Z.T. thanks the support of the Guangdong Innovative Research Team Program (201101C0105067115).

References

1 (*a*) C. W. Tang and S. A. VanSlyke, *Appl. Phys. Lett.*, 1987, **51**, 913; (*b*) C. W. Tang, S. A. VanSlyke and C. H. Chen, *J. Appl. Phys.*, 1989, **65**, 3610.

2 (*a*) J. B. Birks, *Photophysics of Aromatic Molecules*, Wiley, London, UK, 1970; (*b*) I. Capek, *Adv. Colloid Interface Sci.*, 2002, **97**, 91; (*c*) S. W. Thomas III, G. D. Joly and T. M. Swager, *Chem. Rev.*, 2007, **107**, 1339; (*d*) F. Mancin, P. Scrimin, P. Tecilla and U. Tonellato, *Coord. Chem. Rev.*, 2009, **253**, 2150.

3 (*a*) J. Luo, Z. Xie, J. W. Y. Lam, L. Cheng, H. Chen, C. Qiu, H. S. Kwok, X. Zhan, Y. Liu, D. Zhu and B. Z. Tang, *Chem. Commun.*, 2001, 1740; (*b*) B. Z. Tang, X. Zhan, G. Yu, P. P. S. Lee, Y. Liu and D. Zhu, *J. Mater. Chem.*, 2001, **11**, 2974; (*c*) Y. Hong, J. W. Y. Lam and B. Z. Tang, *Chem. Soc. Rev.*, 2011, **40**, 5361; (*d*) Z. Zhao, J. W. Y. Lam and B. Z. Tang, *Curr. Org. Chem.*, 2010, **14**, 2109; (*e*) J. Liu, J. W. Y. Lam and B. Z. Tang, *J. Inorg. Organomet. Polym. Mater.*, 2009, **19**, 249; (*f*) Y. Hong, J. W. Y. Lam and B. Z. Tang, *Chem. Commun.*, 2009, 4332.

4 (*a*) M. Levitus, K. Schmieder, H. Ricks, K. D. Shimizu, U. H. F. Bunz and M. A. Garcia-Garibay, *J. Am. Chem. Soc.*, 2001, **123**, 4259; (*b*) B.-K. An, S.-K. Kwon, S.-D. Jung and S. Y. Park, *J. Am. Chem. Soc.*, 2002, **124**, 14410; (*c*) C. Belton, D. F. O'Brien, W. J. Blau, A. J. Cadby, P. A. Lane, D. D. C. Bradley, H. J. Byrne, R. Stockmann and H.-H. Hörhold, *Appl. Phys. Lett.*, 2001, **78**, 1059; (*d*) L. Antolini, E. Tedesco, G. Barbarella, L. Favaretto, G. Sotgiu, M. Zambianchi, D. Casarini, G. Gigli and R. Cingolani, *J. Am. Chem. Soc.*, 2000, **122**, 9006; (*e*) R. Deans, J. Kim, M. R. Machacek and T. M. Swager, *J. Am. Chem. Soc.*, 2000, **122**, 8565.

5 (*a*) K. Mullen and U. Scherf, *Organic Light-Emitting Devices. Synthesis, Properties and Applications*, Wiley, Weinheim, Germany, 2006; (*b*) J. Roncali, P. Leriche and A. Cravino, *Adv. Mater.*, 2007, **19**, 2045; (*c*) B. Liu, T. T. T. Dan and G. C. Bazan, *Adv. Funct. Mater.*, 2007, **17**, 2432; (*d*) S. H. Yang and C. S. Hsu, *J. Polym. Sci., Part A: Polym. Chem.*, 2008, **46**, 7173.

6 Y. Dong, J. W. Y. Lam, A. Qin, J. Liu, Z. Li and B. Z. Tang, *Appl. Phys. Lett.*, 2007, **91**, 011111.

7 Z. Zhao, C. Y. K. Chan, S. Chen, C. Deng, J. W. Y. Lam, C. K. W. Jim, Y. Hong, P. Lu, Z. Chang, X. Chen, P. Lu, H. S. Kwok, H. Qiu and B. Z. Tang, *J. Mater. Chem.*, 2012, **22**, 4527.

8 Y. Liu, S. Chen, J. W. Y. Lam, P. Lu, R. T. K. Kwok, F. Mahtab, H. S. Kwok and B. Z. Tang, *Chem. Mater.*, 2011, **23**, 2536.

9 Y. Sagara and T. Kato, *Nat. Chem.*, 2009, **1**, 605.

10 (*a*) I. B. Berlman, *Handbook of Fluorescence Spectra of Aromatic Molecules*, Academic Press, New York and London, 1971; (*b*) W. Yuan, P. Lu, S. Chen, J. W. Y. Lam, Z. Wang, Y. Liu, H. S. Kwok, Y. Ma and B. Z. Tang, *Adv. Mater.*, 2010, **22**, 2159.

11 (*a*) H. Tian, J. A. Gan, K. C. Chen, J. He, Q. L. Song and X. Y. Hou, *J. Mater. Chem.*, 2002, **12**, 1262; (*b*) T. Mutai, H. Satou and K. Araki, *Nat. Mater.*, 2005, **4**, 685; (*c*) G. Y. Jiang, S. Wang, W. Yuan, L. Jiang, Y. L. Song, H. Tian and D. B. Zhu, *Chem. Mater.*, 2006, **18**, 235.